Practical Implementation of Delayed Signal Cancellation Method for Phase-Sequence Separation

Jan Svensson, *Member, IEEE*, Massimo Bongiorno, *Student Member, IEEE*, and Ambra Sannino, *Member, IEEE*

***Abstract*—In this paper, the use of a method for online detection of positive- and negative-sequence components of three-phase quantities, named the delayed signal cancellation (DSC) method, is investigated. Problems that arise in practical implementation of the DSC method in computer-controlled systems are investigated. Expressions of the detection error due to nonideal discretization are derived and calculations are verified experimentally. Two methods for reducing the detection error are presented and verified. It is also shown that the given expressions and proposed methods for reducing the detection errors can also be applied to the case of grid frequency variations.**

***Index Terms*—Control, filter, measurement, sequence detection, unbalance, voltage-source converter.**

I. Introduction

EFFECTIVE and robust methods for the detection of positive- and negative-sequence components of voltages and currents are necessary in a vast range of applications using voltage-source converters (VSCs). All kinds of power-conditioning equipment, for example, need accurate information on the positive-sequence voltage in order to achieve unity power factor and load voltage regulation, as well as on the negative-sequence voltage in order to compensate for unbalance conditions. This issue is even more critical when a fast transient response is required, such as in voltage dip compensation by means of the static series compensator (SSC) or dynamic voltage restorer (DVR). Most dips are caused by short-circuit faults, many of which last only a few tens or hundreds of milliseconds and are unbalanced (i.e., involve a negative-sequence component [1]). Hence, the detection system must provide accurate information on the voltage sequence components in a very short time (in the order of milliseconds) for obtaining satisfactory performance. Finally, in many applications in which the VSC provides the interface to the grid, such as wind power plants and many adjustable speed drives, the VSC is often subjected to disturbances that can severely affect its performance and lead to the shutdown of the drive or wind turbine [2]. In many cases, the undesired shutdown can be prevented by designing a more robust current controller, which separately controls positive- and negative-sequence components of the grid voltage [3].

Controllers for the VSC are usually designed in a synchronous reference frame (SRF) (i.e., in a rotating coordinate system synchronized with the grid frequency). A positive-sequence vector appears as a dc component in this frame, while a negative-sequence vector appears as a double-frequency component (i.e., its components oscillate at twice the grid frequency). To isolate the dc component from the double-frequency ripple, filtering techniques may be used. An example is a notch filter with a very deep notch to cut off the oscillatory component of the signal. However, as described in [4], with a high bandwidth for the filter, large transients can be experienced in the estimated sequence components. On the other hand, a low bandwidth for the filter slows down the response.

The method proposed in [5], referred to as delayed signal cancellation (DSC), is considered here. This technique, based on a combination of positive- and negative-sequence component vectors, allows achieving accurate information on sequence components with a time delay of one-quarter of a period (5 ms at 50 Hz). The method has been successfully applied for flicker mitigation by using a shunt-connected VSC [6], series compensation by using a SSC [7], and for shunt-connected VSC used as a front-end rectifier [8].

In this paper, issues concerning the practical application of the DSC method are treated. Implementation in the discrete time domain is studied: the effect of variations in the sampling frequency is analyzed and the consequent error is calculated. Countermeasures to reduce the error in the estimated sequence components are investigated. Moreover, the influence of variations of the grid frequency is analyzed. Simulation and experimental verification of the analytical results are shown and discussed.

II. Principle of the DSC Method

In the general case of an unsymmetrical grid, the grid voltage vector $\underline{e}^{(\alpha\beta)}(t)$ in a fixed two-coordinate system (called $\alpha\beta$ plane) can be written as

$$\underline{e}^{(\alpha\beta)}(t)=\underline{e}_{\mathrm{p}}^{(\alpha\beta)}(t)+\underline{e}_{\mathrm{n}}^{(\alpha\beta)}(t)=E_{\mathrm{p}}\mathrm{e}^{\mathrm{j}(\omega_{\mathrm{g}}t+\varphi_{\mathrm{p}})}+E_{\mathrm{n}}\mathrm{e}^{-\mathrm{j}(\omega_{\mathrm{g}}t+\varphi_{\mathrm{n}})} \tag{1}$$

where E_{p} and E_{n} are the amplitudes of positive and negative phase-sequence voltage vectors, respectively, and φ_{p} and φ_{n} are their phase displacements. The DSC method applied in the $\alpha\beta$ plane is defined by the expressions

$$\underline{\hat{e}}_{\mathrm{p}}^{(\alpha\beta)}(t)=\frac{1}{2}\left[\underline{e}^{(\alpha\beta)}(t)+\mathrm{j}\underline{e}^{(\alpha\beta)}(t-T_{\mathrm{g}}/4)\right] \tag{2}$$

$$\underline{\hat{e}}_{\mathrm{n}}^{(\alpha\beta)}(t)=\frac{1}{2}\left[\underline{e}^{(\alpha\beta)}(t)-\mathrm{j}\underline{e}^{(\alpha\beta)}(t-T_{\mathrm{g}}/4)\right] \tag{3}$$

Manuscript received July 26, 2005; revised January 30, 2006. This work was supported by ELFORSK under the Elektra Program. Paper no. TPWRD-00439-2005.

J. Svensson is with ABB Power Technologies, Västerås SE 72178, Sweden (e-mail: jan.r.svensson@se.abb.com).

M. Bongiorno is with the Division of Electric Power Engineering, Department of Energy and Environment, Chalmers University of Technology, Göteborg 41296, Sweden (e-mail: massimo.bongiorno@chalmers.se).

A. Sannino is with ABB Corporate Research, Power Technologies, Västerås SE 72178, Sweden (e-mail: ambra.sannino@se.abb.com).

Digital Object Identifier 10.1109/TPWRD.2006.881469

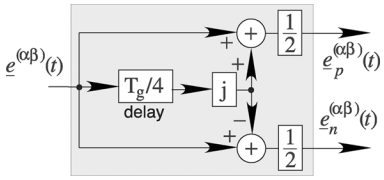

Fig. 1. Block scheme of DSC in continuous time domain.

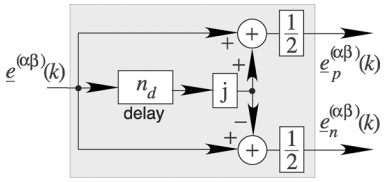

Fig. 2. Block scheme of the DSC in discrete time domain.

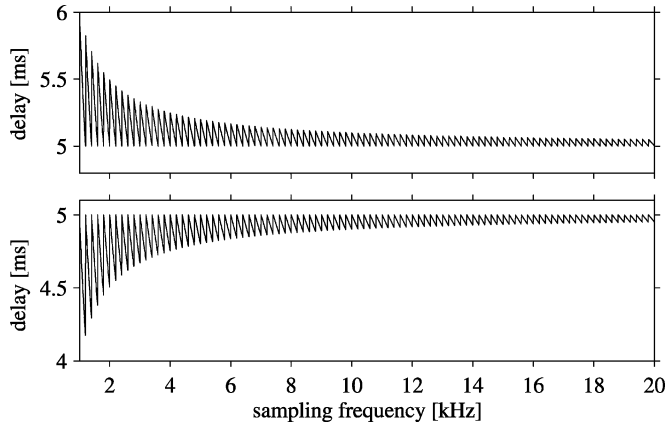

Fig. 3. Time delay as a function of sampling frequency for fixed grid frequency ($f_g = 50$ Hz). Top: Delay rounded up to the nearest higher integer n_{d2}. Bottom: Delay rounded down to the nearest lower integer n_{d1}.

where $\hat{\underline{e}}_p^{(\alpha\beta)}(t)$ and $\hat{\underline{e}}_n^{(\alpha\beta)}(t)$ are the estimated positive and negative phase-sequence voltages, respectively, and T_g is the period of the grid voltage. The block scheme of the DSC is shown in Fig. 1. It is straightforward to verify that, by substituting (1) into (2) and (3), the estimated phase-sequence voltage vectors result in

$$\hat{\underline{e}}_p^{(\alpha\beta)}(t) = E_p e^{j(\omega_g t+\varphi_p)} \quad (4)$$

$$\hat{\underline{e}}_n^{(\alpha\beta)}(t) = E_n e^{-j(\omega_g t+\varphi_n)} \quad (5)$$

(i.e., equal to the corresponding sequence voltage vectors). The method implies delaying the signal by one-quarter of period at the fundamental frequency, which then constitutes its inherent time delay.

III. Digital Implementation of the DSC Method

A. Influence of Sampling Frequency

Equations (2) and (3), defining the DSC method, are expressed in the continuous time domain. However, to be implemented in a computer-controlled system as is necessary in most practical applications, the method has to be expressed in the discrete time domain. The block scheme of the discrete DSC is shown in Fig. 2. Assuming a sampling frequency equal to f_s, (2) and (3) can be rewritten in the discrete time domain as

$$\hat{\underline{e}}_p^{(\alpha\beta)}(kT_s) = \frac{1}{2}\left[\underline{e}^{(\alpha\beta)}(kT_s) + j\underline{e}^{(\alpha\beta)}(kT_s - n_d T_s)\right] \quad (6)$$

$$\hat{\underline{e}}_n^{(\alpha\beta)}(kT_s) = \frac{1}{2}\left[\underline{e}^{(\alpha\beta)}(kT_s) - j\underline{e}^{(\alpha\beta)}(kT_s - n_d T_s)\right] \quad (7)$$

where $T_s = 1/f_s$ is the sampling time and the delay n_d, expressed as a number of samples, is equal to

$$n_d = f_s/4f_g. \quad (8)$$

Ideally, the sampling frequency should be chosen so that n_d resulting from (8) is an integer. Unfortunately, the value of the switching frequency (and, consequently, of the sampling frequency) is normally selected based on other considerations. This may result in a nonideal sample delay, which occurs if the result from (8) is not an integer. In this case, if the sampling frequency is set and the grid frequency is constant, the result of (8) must be rounded off to the nearest lower or higher integer, denoted by n_{d1} and n_{d2}, respectively. This results in a time delay equal to or smaller than the correct value, or in a time delay equal or larger than the correct value, respectively. This is shown in Fig. 3 for different values of the sampling frequency.

B. Error Calculation

The expression of the detection error introduced by the nonideal delay time due to discretization will now be calculated. The discrete time delay can be written as

$$n_d T_s = T_c + \Delta T \quad (9)$$

(i.e., as the sum of the correct time delay T_c), equal to $T_g/4$, and a time delay error ΔT. Substituting (9) into (6), the estimated positive-sequence component $\hat{\underline{e}}_p^{(\alpha\beta)}(kT_s)$ can be expressed as

$$\begin{aligned}\hat{\underline{e}}_p^{(\alpha\beta)}(kT_s) = \frac{1}{2}&\left[E_p e^{j(\omega_g kT_s+\varphi_p)} + E_n e^{-j(\omega_g kT_s+\varphi_n)}\right] \\ &+ j\frac{1}{2}\left[E_p e^{j(\omega_g(kT_s-T_c)+\varphi_p)} e^{-j(\omega_g \Delta T)}\right. \\ &\left. + E_n e^{-j(\omega_g(kT_s-T_c)+\varphi_n)} e^{j(\omega_g \Delta T)}\right] \quad (10)\end{aligned}$$

which can be further simplified to obtain

$$\begin{aligned}\hat{\underline{e}}_p^{(\alpha\beta)}(kT_s) = \underline{e}_p^{(\alpha\beta)}(kT_s) &+ E_p\lambda e^{j\left(\omega_g kT_s - \frac{\pi}{2}+\varphi_p+\gamma\right)} \\ &+ E_n\lambda e^{-j\left(\omega_g kT_s - \frac{\pi}{2}+\varphi_n+\gamma\right)} \quad (11)\end{aligned}$$

where

$$\lambda = \sqrt{\frac{1}{2}\left(1 - \cos\left(\frac{\pi}{2}\kappa\right)\right)} \quad (12)$$

and

$$\gamma = \arctan\left[\frac{\cos\left(\frac{\pi}{2}\kappa\right) - 1}{\sin\left(\frac{\pi}{2}\kappa\right)}\right]. \quad (13)$$

In (12) and (13), κ is the relative time error, defined by

$$\kappa = \Delta T/T_c. \quad (14)$$

From (11), the estimation error for the positive-sequence component is

$$\Delta\underline{e}_{\mathrm{p}}^{(\alpha\beta)}(kT_{\mathrm{s}}) = E_{\mathrm{p}}\lambda \mathrm{e}^{\mathrm{j}\left(\omega_{\mathrm{g}}kT_{\mathrm{s}}-\frac{\pi}{2}+\varphi_{\mathrm{p}}+\gamma\right)} + E_{\mathrm{n}}\lambda \mathrm{e}^{-\mathrm{j}\left(\omega_{\mathrm{g}}kT_{\mathrm{s}}-\frac{\pi}{2}+\varphi_{\mathrm{n}}+\gamma\right)}. \quad (15)$$

Similarly, the estimation error for the negative-sequence detection algorithm can be expressed as

$$\Delta\underline{e}_{\mathrm{n}}^{(\alpha\beta)}(kT_{\mathrm{s}}) = E_{\mathrm{p}}\lambda \mathrm{e}^{\mathrm{j}\left(\omega_{\mathrm{g}}kT_{\mathrm{s}}-\frac{\pi}{2}+\varphi_{\mathrm{p}}-\gamma\right)} + E_{\mathrm{n}}\lambda \mathrm{e}^{-\mathrm{j}\left(\omega_{\mathrm{g}}kT_{\mathrm{s}}-\frac{\pi}{2}+\varphi_{\mathrm{n}}-\gamma\right)}. \quad (16)$$

By applying the transformation

$$\underline{e}_{\mathrm{p}}^{(dqp)}(kT_{\mathrm{s}}) = \underline{e}_{\mathrm{p}}^{(\alpha\beta)}(kT_{\mathrm{s}})\mathrm{e}^{-\mathrm{j}(\omega_{\mathrm{g}}kT_{\mathrm{s}})} \quad (17)$$

the estimated positive-sequence component in (10) can be transformed into a positively-rotating SRF (dqp-frame) where the voltage vector is aligned with the direction of the d-axis during steady state. The estimation error for the positive-sequence voltage in the dqp-coordinate system results as

$$\begin{aligned}\Delta\underline{e}_{\mathrm{p}}^{(dqp)}(kT_{\mathrm{s}}) &= E_{\mathrm{p}}\lambda \mathrm{e}^{\mathrm{j}\left(\varphi_{\mathrm{p}}+\gamma-\frac{\pi}{2}\right)} + E_{\mathrm{n}}\lambda \mathrm{e}^{-\mathrm{j}\left(2\omega_{\mathrm{g}}kT_{\mathrm{s}}-\frac{\pi}{2}+\varphi_{\mathrm{n}}+\gamma\right)} \\ &= \Delta\underline{e}_{\mathrm{p,off}}^{(dqp)} + \Delta\underline{e}_{\mathrm{p,osc}}^{(dqp)}\cos(2\omega_{\mathrm{g}}kT_{\mathrm{s}} - \delta_{\mathrm{p}}) \quad (18)\end{aligned}$$

which contains a constant term (offset, denoted as $\Delta\underline{e}_{\mathrm{p,off}}^{(dqp)}$) and a fluctuating part ($\Delta\underline{e}_{\mathrm{p,osc}}^{(dqp)}$), oscillating at twice the grid frequency. The same holds for the negative-sequence component, which is transformed into a negatively rotating SRF by using the transformation

$$\underline{e}_{\mathrm{n}}^{(dqn)}(kT_{\mathrm{s}}) = \underline{e}_{\mathrm{n}}^{(\alpha\beta)}(kT_{\mathrm{s}})\mathrm{e}^{\mathrm{j}(\omega_{\mathrm{g}}kT_{\mathrm{s}})} \quad (19)$$

yielding

$$\begin{aligned}\Delta\underline{e}_{\mathrm{n}}^{(dqn)}(kT_{\mathrm{s}}) &= E_{\mathrm{p}}\lambda \mathrm{e}^{\mathrm{j}\left(2\omega_{\mathrm{g}}kT_{\mathrm{s}}-\frac{\pi}{2}+\varphi_{\mathrm{p}}-\gamma\right)} + E_{\mathrm{n}}\lambda \mathrm{e}^{-\mathrm{j}\left(\varphi_{\mathrm{n}}-\gamma-\frac{\pi}{2}\right)} \\ &= \Delta\underline{e}_{\mathrm{n,osc}}^{(dqn)}\cos(2\omega_{\mathrm{g}}kT_{\mathrm{s}} - \delta_{\mathrm{n}}) + \Delta\underline{e}_{\mathrm{n,off}}^{(dqn)}. \quad (20)\end{aligned}$$

Equations (18) and (20) can further be separated into their components, yielding, for example, for the positive-sequence d- and q-components

$$\Delta\underline{e}_{\mathrm{p}d}^{(dqp)}(kT_{\mathrm{s}}) = \Delta\underline{e}_{\mathrm{p}d,\mathrm{off}}^{(dqp)} + \Delta\underline{e}_{\mathrm{p}d,\mathrm{osc}}^{(dqp)}\cos(2\omega_{\mathrm{g}}kT_{\mathrm{s}} - \delta_{\mathrm{p}d}) \quad (21)$$

$$\Delta\underline{e}_{\mathrm{p}q}^{(dqp)}(kT_{\mathrm{s}}) = \Delta\underline{e}_{\mathrm{p}q,\mathrm{off}}^{(dqp)} + \Delta\underline{e}_{\mathrm{p}q,\mathrm{osc}}^{(dqp)}\cos(2\omega_{\mathrm{g}}kT_{\mathrm{s}} - \delta_{\mathrm{p}q}) \quad (22)$$

and, similarly, for the negative sequence

$$\Delta\underline{e}_{\mathrm{n}d}^{(dqn)}(kT_{\mathrm{s}}) = \Delta\underline{e}_{\mathrm{n}d,\mathrm{off}}^{(dqn)} + \Delta\underline{e}_{\mathrm{n}d,\mathrm{osc}}^{(dqn)}\cos(2\omega_{\mathrm{g}}kT_{\mathrm{s}} - \delta_{\mathrm{n}d}) \quad (23)$$

$$\Delta\underline{e}_{\mathrm{n}q}^{(dqn)}(kT_{\mathrm{s}}) = \Delta\underline{e}_{\mathrm{n}q,\mathrm{off}}^{(dqn)} + \Delta\underline{e}_{\mathrm{n}q,\mathrm{osc}}^{(dqn)}\cos(2\omega_{\mathrm{g}}kT_{\mathrm{s}} - \delta_{\mathrm{n}q}). \quad (24)$$

C. Detection Error Due to Rounding

The time delay due to discretization can be written as

$$n_{\mathrm{d}1}T_{\mathrm{s}} = T_{\mathrm{c}} + \Delta T_1 \quad (25)$$

$$n_{\mathrm{d}2}T_{\mathrm{s}} = T_{\mathrm{c}} + \Delta T_2 \quad (26)$$

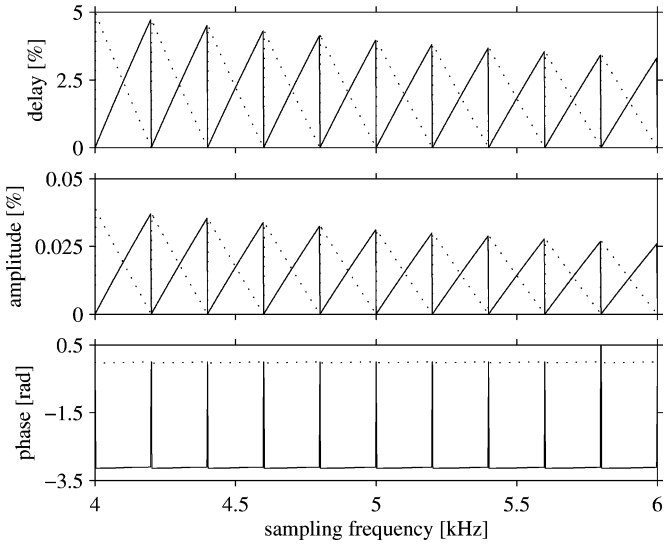

Fig. 4. Top: Absolute value of relative time delay error obtained by rounding down (κ_1, solid) or up (κ_2, dotted) to the nearest integer. Middle: Amplitude of relative estimation error for System 1 (λ_1, solid) and System 2 (λ_2, dotted). Bottom: Phase of the relative estimation error for System 1 (γ_1, solid) and System 2 (γ_2, dotted). Grid frequency $f_{\mathrm{g}} = 50$ Hz.

when rounding down or up to the nearest integer, respectively. Thus, $\Delta T_1 < 0$ and $\Delta T_2 > 0$. The positive- and negative-sequence estimation errors for "System 1" using ΔT_1 are indicated as $\Delta\underline{e}_{\mathrm{p1}}^{(\alpha\beta)}(kT_{\mathrm{s}})$ and $\Delta\underline{e}_{\mathrm{n1}}^{(\alpha\beta)}(kT_{\mathrm{s}})$, respectively. These are obtained by replacing λ and γ in (15) and (16) with λ_1 and γ_1, obtained from (12) and (13) with $\kappa = \kappa_1 = \Delta T_1/T_{\mathrm{c}}$. The errors in the dqp- and dqn-frame $\Delta\underline{e}_{\mathrm{p1}}^{(dqp)}(kT_{\mathrm{s}})$ and $\Delta\underline{e}_{\mathrm{n1}}^{(dqn)}(kT_{\mathrm{s}})$ are obtained similarly from (18) and (20). The same formulation holds as in (21)–(24) for the components, with an additional subscript "1" for System 1.

For "System 2," which uses ΔT_2, the positive- and negative-sequence estimation errors $\Delta\underline{e}_{\mathrm{p2}}^{(\alpha\beta)}(kT_{\mathrm{s}})$ and $\Delta\underline{e}_{\mathrm{n2}}^{(\alpha\beta)}(kT_{\mathrm{s}})$ have analogous expressions, with λ_1 and γ_1 replaced by λ_2 and γ_2, obtained from (12) and (13) with $\kappa = \kappa_2 = \Delta T_2/T_{\mathrm{c}}$. The same holds for the errors in the positive and negative SFRs and their components.

Fig. 4 shows the amplitude and phase of the positive-sequence estimation error when rounding up or down to the nearest integer. The amplitudes λ_1 and λ_2 of the error are equal when f_{s} is an even multiple of f_{g}, in particular, being zero when f_{s} is a multiple of $4f_{\mathrm{g}}$, as expected. Otherwise, the amplitude of the error is lowest for the lowest relative time error κ.

IV. Experimental Verification

In order to demonstrate the validity of the previous derivation, experimental results are presented in this section. Measurements have been carried out both with balanced and unbalanced voltage.

A. Laboratory Setup

A scheme of the experimental setup is displayed in Fig. 5. The setup consists of an analog 400-V grid model and a control computer, dSPACE 1103 [9]. The analog model consists of six identical Π-sections connected in series, each constituted by a series inductor of 2.05 mH and two shunt capacitors of 46 μF.

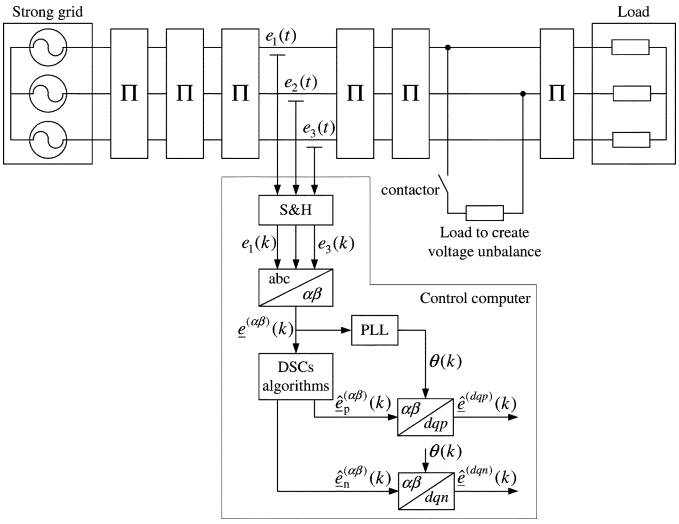

Fig. 5. Scheme of laboratory setup and controller algorithm.

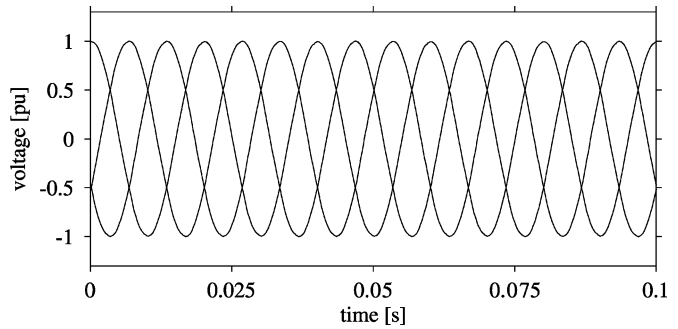

Fig. 6. Measured balanced three-phase grid voltages.

The model is loaded with a three-phase resistor of 8.8 Ω (18 kW). In order to generate unbalanced voltage at the measurement point, an additional resistor of 4.2 Ω was connected between phases 1 and 2 by closing a contactor (shown in Fig. 5).

The measured phase voltages are sampled and transformed into the fixed $\alpha\beta$-plane obtaining $\underline{e}^{(\alpha\beta)}(k)$, used as input to the DSC algorithm. Estimated positive- and negative-sequence components of the grid voltage are then transformed into the corresponding rotating SRFs. The phase-locked loop (PLL) [10] is synchronized with the grid voltage vector $\underline{e}^{(\alpha\beta)}(k)$ and the transformation angle, denoted as $\theta(k)$, is equal to the grid voltage angle in steady state. The bandwidth of the phase-locked loop (PLL) is set to 30 rad/s, so that it tracks the fundamental component of the grid voltage without sensing the harmonics [11].

B. Balanced Grid Voltage

A first set of tests was carried out during steady state, with balanced voltage at nominal value. The measured three-phase voltages are shown in Fig. 6. The measured grid frequency is approximately 50 Hz, while the sampling frequency is set to 5060 Hz. In these conditions, $n_{\rm d} = 25.3$. The relevant parameters for System 1 and 2 are given in Table I. The error components in (21)–(24) are calculated for System 1 and 2 and reported in Tables II and III, respectively. The measured error of the estimated positive- and negative-sequence components of the grid voltage, plotted in Figs. 7 and 8 for System 1 and 2, respectively, confirm the calculations above. As shown, the error is larger for System 2 due to higher λ.

TABLE I
DSC PARAMETERS FOR SYSTEM 1 AND 2 FOR STUDY CASE

$E_{\rm p} = 1.0$ pu	$E_{\rm n} = 0$ pu	$\varphi_{\rm p} = 0°$	$\varphi_{\rm n} = 0°$
System 1			
$n_{\rm d1} = 25$	$\kappa_1 = -1.19\%$	$\lambda_1 = 0.93\%$	$\gamma_1 = 180.5°$
System 2			
$n_{\rm d2} = 26$	$\kappa_2 = 2.77\%$	$\lambda_2 = 2.17\%$	$\gamma_2 = 358.8°$

TABLE II
COMPONENTS OF DETECTION ERROR FOR STUDY CASE WITH BALANCED VOLTAGE, SYSTEM 1

Positive sequence					
$\Delta e_{\rm pd1,off}^{(dqp)}$	-0.01%	$\Delta e_{\rm pd1,osc}^{(dqp)}$	0%	$\delta_{\rm pd1}$	-
$\Delta e_{\rm pq1,off}^{(dqp)}$	0.93%	$\Delta e_{\rm pq1,osc}^{(dqp)}$	0%	$\delta_{\rm pq1}$	-
Negative sequence					
$\Delta e_{\rm nd1,off}^{(dqn)}$	0%	$\Delta e_{\rm nd1,osc}^{(dqn)}$	0.93%	$\delta_{\rm nd1}$	$270.5°$
$\Delta e_{\rm nq1,off}^{(dqn)}$	0%	$\Delta e_{\rm nq1,osc}^{(dqn)}$	0.93%	$\delta_{\rm nq1}$	$0.5°$

TABLE III
COMPONENTS OF DETECTION ERROR FOR STUDY CASE WITH BALANCED VOLTAGE, SYSTEM 2

Positive sequence					
$\Delta e_{\rm pd2,off}^{(dqp)}$	-0.05%	$\Delta e_{\rm pd2,osc}^{(dqp)}$	0%	$\delta_{\rm pd2}$	-
$\Delta e_{\rm pq2,off}^{(dqp)}$	-2.17%	$\Delta e_{\rm pq2,osc}^{(dqp)}$	0%	$\delta_{\rm pq2}$	-
Negative sequence					
$\Delta e_{\rm nd2,off}^{(dqn)}$	0%	$\Delta e_{\rm nd2,osc}^{(dqn)}$	2.17%	$\delta_{\rm nd2}$	$88.8°$
$\Delta e_{\rm nq2,off}^{(dqn)}$	0%	$\Delta e_{\rm nq2,osc}^{(dqn)}$	2.17%	$\delta_{\rm nq2}$	$178.8°$

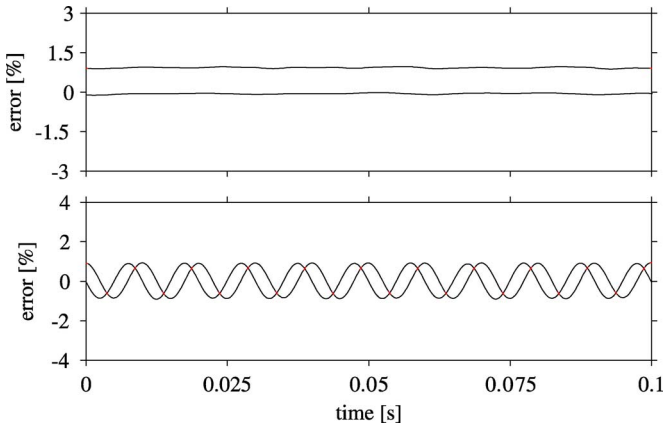

Fig. 7. Measured error in phase-sequence estimation with balanced steady-state voltage using System 1 $f_{\rm g} = 50$ Hz, $f_{\rm s} = 5060$ Hz. Top: Positive-sequence components in positive SRF (black: d-component; red: q-component). Bottom: Negative-sequence components in negative SRF (black: d-component; red: q-component).

C. Unbalanced Grid Voltage

Further tests have been carried out with the same sampling frequency under unbalanced grid conditions. The unbalanced current circulating in the Π sections of the network model creates the three-phase voltages in Fig. 9. The measured sequence components of the grid voltage are $E_{\rm p} = 0.896$ p.u. and $E_{\rm n} = 0.058$ p.u., corresponding to a degree of unbalance $E_{\rm n}/E_{\rm p} =$

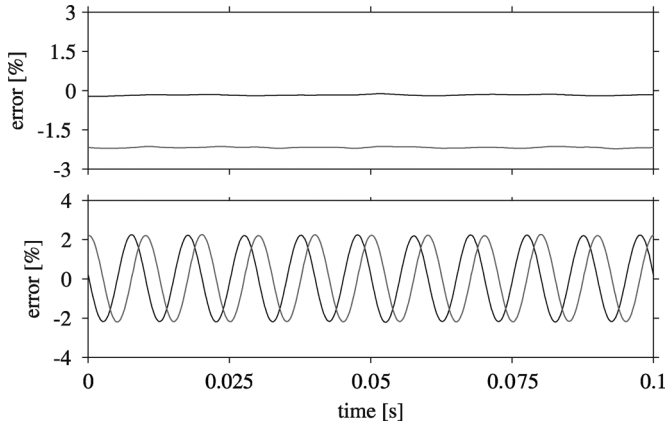

Fig. 8. Measured error in phase-sequence estimation with balanced steady-state voltage using System 2 $f_{\rm g} = 50$ Hz, $f_{\rm s} = 5060$ Hz. Top: Positive-sequence components in positive SRF (black: d-component; red: q-component). Bottom: Negative-sequence components in negative SRF (black: d-component; red: q-component).

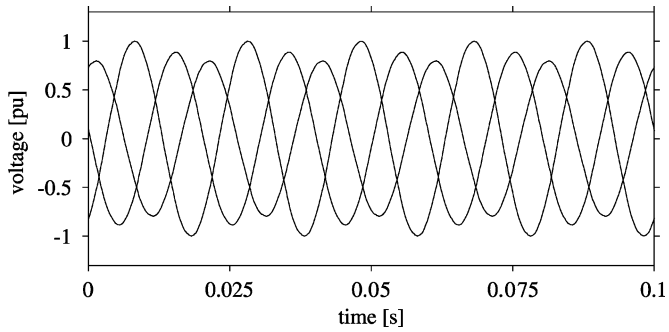

Fig. 9. Measured unbalanced three-phase grid voltages.

TABLE IV
CALCULATED COMPONENTS OF DETECTION ERROR FOR STUDY CASE WITH UNBALANCED VOLTAGE, SYSTEM 1

Positive sequence					
$\Delta e^{(dqp)}_{\rm pd1,off}$	-0.01%	$\Delta e^{(dqp)}_{\rm pd1,osc}$	0.05%	$\delta_{\rm pd1}$	$176.7°$
$\Delta e^{(dqp)}_{\rm pq1,off}$	0.83%	$\Delta e^{(dqp)}_{\rm pq1,osc}$	0.05%	$\delta_{\rm pq1}$	$86.7°$
Negative sequence					
$\Delta e^{(dqn)}_{\rm nd1,off}$	-0.05%	$\Delta e^{(dqn)}_{\rm nd1,osc}$	0.84%	$\delta_{\rm nd1}$	$270.5°$
$\Delta e^{(dqn)}_{\rm nq1,off}$	0.002%	$\Delta e^{(dqn)}_{\rm nq1,osc}$	0.84%	$\delta_{\rm nq1}$	$0.5°$

6.49%. As for the balanced case, the positive-sequence voltage vector is taken as reference, thus $\varphi_{\rm p} = 0°$. For the negative sequence, $\varphi_{\rm n} = 92.8°$.

The voltage unbalance, together with nonideal sampling frequency, results in additional oscillatory error for the positive-sequence voltage. Calculated components of the detection error for System 1 and 2 are shown in Tables IV and V, respectively. The calculated errors displayed in Table IV can be compared with the measured errors of the estimated components of the grid voltage in the corresponding SRFs, displayed in Fig. 10 for System 1. It is of interest to observe that the oscillations in the measured error in the estimated positive-sequence components are not constant, which is in disagreement with (18). These oscillations present a maximum peak-to-peak value of 0.14% and a minimum value of 0.12%. This is because the analysis has been carried out assuming the ideal supply voltage and accurate knowledge of the grid voltage angle. However, in a real system, the supply voltage is affected by low-order harmonics, which results in an error in the estimated grid voltage angle [12], leading to a modulated signal in the dq-coordinate system. Analogous results have been obtained using System 2, as shown in Fig. 11.

TABLE V
CALCULATED COMPONENTS OF DETECTION ERROR FOR STUDY CASE WITH UNBALANCED VOLTAGE, SYSTEM 2

Positive sequence					
$\Delta e^{(dqp)}_{\rm pd2,off}$	-0.04%	$\Delta e^{(dqp)}_{\rm pd2,osc}$	0.13%	$\delta_{\rm pd2}$	$358.4°$
$\Delta e^{(dqp)}_{\rm pq2,off}$	-1.95%	$\Delta e^{(dqp)}_{\rm pq2,osc}$	0.13%	$\delta_{\rm pq2}$	$268.4°$
Negative sequence					
$\Delta e^{(dqn)}_{\rm nd2,off}$	0.13%	$\Delta e^{(dqn)}_{\rm nd2,osc}$	1.95%	$\delta_{\rm nd2}$	$88.8°$
$\Delta e^{(dqn)}_{\rm nq2,off}$	-0.01%	$\Delta e^{(dqn)}_{\rm nq2,osc}$	1.95%	$\delta_{\rm nq2}$	$178.8°$

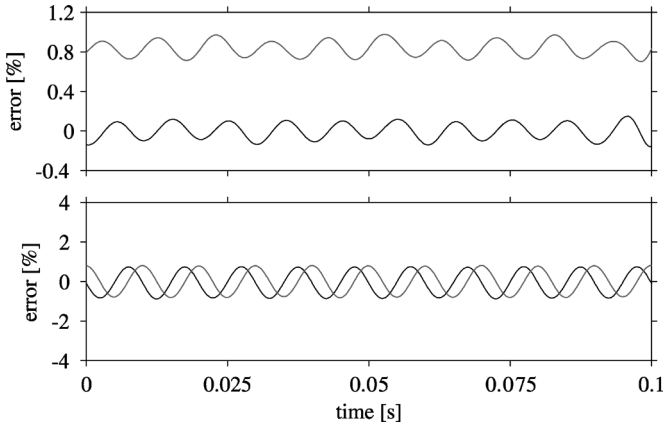

Fig. 10. Measured error in phase-sequence estimation with unbalanced steady-state voltage using System 1 $f_{\rm g} = 50$ Hz, $f_{\rm s} = 5060$ Hz. Top: Positive-sequence components in positive SRF (black: d-component; red: q-component). Bottom: Negative-sequence components in negative SRF (black: d-component; red: q-component).

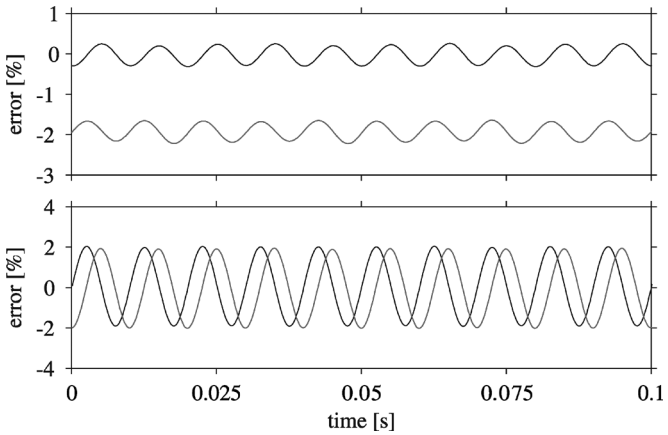

Fig. 11. Measured error in phase-sequence estimation with unbalanced steady-state voltage using System 2 $f_{\rm g} = 50$ Hz, $f_{\rm s} = 5060$ Hz. Top: Positive-sequence components in positive SRF (black: d-component; red: q-component). Bottom: Negative-sequence components in negative SRF (black: d-component; red: q-component).

V. Methods to Reduce the Detection Error

A. Reduction of Detection Error by Average Value

The variation of the error with the sampling frequency seen in Fig. 4 suggests the error can be reduced by averaging. Consider the average error defined as

$$\Delta \underline{e}_{\mathrm{p,av}}^{(\alpha\beta)}(kT_\mathrm{s}) = \frac{1}{2}\left[\Delta \underline{e}_{\mathrm{p1}}^{(\alpha\beta)}(kT_\mathrm{s}) + \Delta \underline{e}_{\mathrm{p2}}^{(\alpha\beta)}(kT_\mathrm{s})\right] \quad (27)$$

for the positive sequence and, similarly, as

$$\Delta \underline{e}_{\mathrm{n,av}}^{(\alpha\beta)}(kT_\mathrm{s}) = \frac{1}{2}\left[\Delta \underline{e}_{\mathrm{n1}}^{(\alpha\beta)}(kT_\mathrm{s}) + \Delta \underline{e}_{\mathrm{n2}}^{(\alpha\beta)}(kT_\mathrm{s})\right] \quad (28)$$

for the negative sequence. By substituting (15) for System 1 and 2 into (27), the average error for the positive-sequence results after some rewriting as

$$\Delta \underline{e}_{\mathrm{p,av}}^{(\alpha\beta)}(kT_\mathrm{s}) = E_\mathrm{p}\mathrm{e}^{\mathrm{j}\left(\omega_\mathrm{g}kT_\mathrm{s}-\frac{\pi}{2}+\varphi_\mathrm{p}\right)}\lambda_\mathrm{av}\mathrm{e}^{\mathrm{j}\gamma_\mathrm{av}} + E_\mathrm{n}\mathrm{e}^{-\mathrm{j}\left(\omega_\mathrm{g}kT_\mathrm{s}-\frac{\pi}{2}+\varphi_\mathrm{n}\right)}\lambda_\mathrm{av}\mathrm{e}^{-\mathrm{j}\gamma_\mathrm{av}} \quad (29)$$

with

$$\lambda_\mathrm{av} = \frac{1}{2}\sqrt{[\lambda_1^2+\lambda_2^2+2\lambda_1\lambda_2\cos(\gamma_1-\gamma_2)]} \quad (30)$$

$$\gamma_\mathrm{av} = \arctan\left(\frac{\lambda_1\sin\gamma_1+\lambda_2\sin\gamma_2}{\lambda_1\cos\gamma_1+\lambda_2\cos\gamma_2}\right). \quad (31)$$

Let the system characterized by λ_av and γ_av be called "System 3." By using (12) and (13), (30) and (31) can be rewritten as

$$\lambda_\mathrm{av} = \sqrt{\frac{1}{8}\left[3-2\cos\frac{\pi}{2}\kappa_1-2\cos\frac{\pi}{2}\kappa_2+\cos\frac{\pi}{2}(\kappa_1-\kappa_2)\right]} \quad (32)$$

$$\gamma_\mathrm{av} = \arctan\left(\frac{\cos\frac{\pi}{2}\kappa_1+\cos\frac{\pi}{2}\kappa_2-2}{\sin\frac{\pi}{2}\kappa_1+\sin\frac{\pi}{2}\kappa_2}\right). \quad (33)$$

Fig. 12 shows amplitude and phase of the positive-sequence estimation error for System 1, 2, and 3. There is a rather large range of frequencies for which the average error λ_av is considerably lower than λ_1 and λ_2. Averaging should thus lead to reduce the detection error due to discretization.

Equation (29) can be further written in the positive SRF as

$$\Delta \underline{e}_{\mathrm{p,av}}^{(dqp)}(kT_\mathrm{s}) = E_\mathrm{p}\lambda_\mathrm{av}\mathrm{e}^{\mathrm{j}\left(\varphi_\mathrm{p}+\gamma_\mathrm{av}-\frac{\pi}{2}\right)} + E_\mathrm{n}\lambda_\mathrm{av}\mathrm{e}^{-\mathrm{j}\left(2\omega_\mathrm{g}kT_\mathrm{s}-\frac{\pi}{2}+\varphi_\mathrm{n}+\gamma_\mathrm{av}\right)}. \quad (34)$$

With similar derivation, the average error for the negative sequence in the negatively rotating SRF can be expressed as

$$\Delta \underline{e}_{\mathrm{n,av}}^{(dqn)}(kT_\mathrm{s}) = E_\mathrm{p}\lambda_\mathrm{av}\mathrm{e}^{\mathrm{j}\left(2\omega_\mathrm{g}kT_\mathrm{s}-\frac{\pi}{2}+\varphi_\mathrm{p}-\gamma_\mathrm{av}\right)} + E_\mathrm{n}\lambda_\mathrm{av}\mathrm{e}^{-\mathrm{j}\left(\varphi_\mathrm{n}-\gamma_\mathrm{av}-\frac{\pi}{2}\right)}. \quad (35)$$

Similar expressions as in (21)–(24) hold for the components, with an additional subscript "av" indicating System 3.

B. Reduction of Detection Error by Weighted Mean Value

When using weighted mean averaging, the error is defined as

$$\Delta \underline{e}_{\mathrm{p,w}}^{(\alpha\beta)}(kT_\mathrm{s}) = a\Delta \underline{e}_{\mathrm{p1}}^{(\alpha\beta)}(kT_\mathrm{s}) + (1-a)\Delta \underline{e}_{\mathrm{p2}}^{(\alpha\beta)}(kT_\mathrm{s}) \quad (36)$$

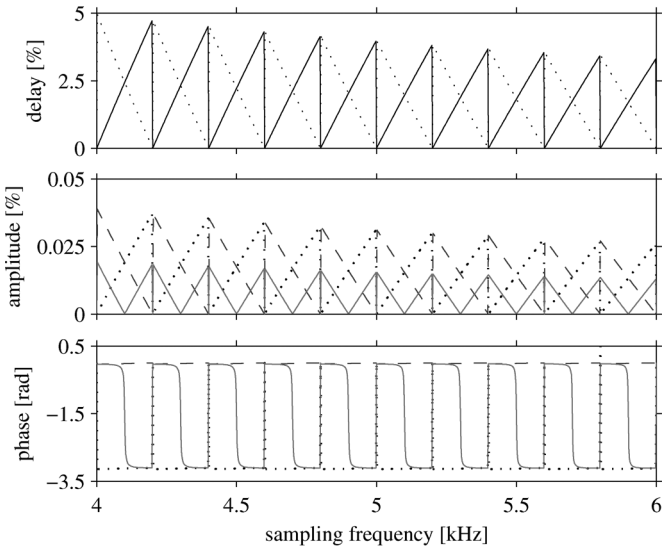

Fig. 12. Top: relative time delay error obtained by rounding down (κ_1, solid) or up (κ_2, dotted) to nearest integer. Middle: amplitude of relative estimation error for System 1 (λ_1, black dotted), System 2 (λ_2, blue dashed) and System 3 (λ_av, solid). Bottom: phase of relative estimation error for System 1 (γ_1, black dotted), System 2 (γ_2, blue dashed) and System 3 (γ_av, solid).

for the positive sequence and

$$\Delta \underline{e}_{\mathrm{n,w}}^{(\alpha\beta)}(kT_\mathrm{s}) = a\Delta \underline{e}_{\mathrm{n1}}^{(\alpha\beta)}(kT_\mathrm{s}) + (1-a)\Delta \underline{e}_{\mathrm{n2}}^{(\alpha\beta)}(kT_\mathrm{s}) \quad (37)$$

for the negative sequence, where the parameter $0 \le a \le 1$ is chosen to minimize the error, which depends on ΔT_1 and ΔT_2. To reduce the complexity of the coming derivation, the delay error Δn, defined as $\Delta n = -\Delta T_1/T_\mathrm{s} = 1 - \Delta T_2/T_\mathrm{s}$, is used. The relative time errors become

$$\kappa_1 = n_\mathrm{d1}/(n_\mathrm{d1}+\Delta n) - 1 \quad (38)$$

$$\kappa_2 = (n_\mathrm{d1}+1)/(n_\mathrm{d1}+\Delta n) - 1. \quad (39)$$

The positive-sequence error in (36) is rewritten as

$$\Delta \underline{e}_{\mathrm{p,w}}^{(\alpha\beta)}(kT_\mathrm{s}) = E_\mathrm{p}\mathrm{e}^{\mathrm{j}\left(\omega_\mathrm{g}kT_\mathrm{s}-\frac{\pi}{2}+\varphi_\mathrm{p}\right)}\lambda_\mathrm{w}\mathrm{e}^{\mathrm{j}\gamma_\mathrm{w}} + E_\mathrm{n}\mathrm{e}^{-\mathrm{j}\left(\omega_\mathrm{g}kT_\mathrm{s}-\frac{\pi}{2}+\varphi_\mathrm{p}\right)}\lambda_\mathrm{w}\mathrm{e}^{-\mathrm{j}\gamma_\mathrm{w}} \quad (40)$$

where the amplitude and phase error λ_w and γ_w are a function of n_d1, Δn and a. To find the value of a that minimizes λ_w for each n_d1 and Δn, the derivative of λ_w is nullified. The obtained expression for the parameter a can then be simplified using Taylor expansion and considering the first term only, giving

$$a = 1 - \Delta n. \quad (41)$$

Amplitude and phase of the relative estimation error λ_w and γ_w can be written as (42)–(43), shown at the bottom of the next page, where

$$\upsilon_1 = \frac{\pi}{2}\frac{n_\mathrm{d1}}{n_\mathrm{d1}+\Delta n} \quad \upsilon_2 = \frac{\pi}{2}\frac{n_\mathrm{d1}+1}{n_\mathrm{d1}+\Delta n}.$$

It is of interest to observe that the maximum error in λ_w is less than 0.2% when $f_\mathrm{s}/f_\mathrm{g} \geqslant 16$. As shown in Fig. 13, the error decreases quickly with increasing n_d1.

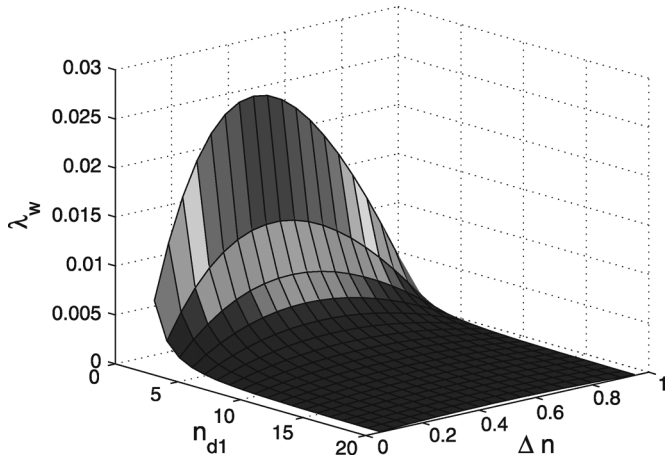

Fig. 13. Trend of λ_{w} as a function of Δn and n_{d1}.

Similar to the previous sections, the estimated weighted error for the positive and negative sequences in the corresponding rotating SRF is derived as

$$\Delta \underline{e}_{\mathrm{p,w}}^{(dqp)}(kT_{\mathrm{s}}) = E_{\mathrm{p}}\lambda_{\mathrm{w}}\mathrm{e}^{\mathrm{j}\left(\varphi_{\mathrm{p}}+\gamma_{\mathrm{w}}-\frac{\pi}{2}\right)} + E_{\mathrm{n}}\lambda_{\mathrm{w}}\mathrm{e}^{-\mathrm{j}\left(2\omega_{\mathrm{g}}kT_{\mathrm{s}}-\frac{\pi}{2}+\varphi_{\mathrm{n}}+\gamma_{\mathrm{w}}\right)} \quad (44)$$

$$\Delta \underline{e}_{\mathrm{n,w}}^{(dqn)}(kT_{\mathrm{s}}) = E_{\mathrm{p}}\lambda_{\mathrm{w}}\mathrm{e}^{\mathrm{j}\left(2\omega_{\mathrm{g}}kT_{\mathrm{s}}-\frac{\pi}{2}+\varphi_{\mathrm{p}}-\gamma_{\mathrm{w}}\right)} + E_{\mathrm{n}}\lambda_{\mathrm{w}}\mathrm{e}^{-\mathrm{j}\left(\varphi_{\mathrm{n}}-\gamma_{\mathrm{w}}-\frac{\pi}{2}\right)}. \quad (45)$$

Similar expressions as in (21)–(24) hold for the error components, with the additional subscript "w" indicating System 4.

VI. Experimental Verification Using Averaging and Weighted Mean Averaging

The proposed methods have been tested experimentally under the same unbalanced condition of the grid voltage as in Section IV-C. DSC parameters and calculated components of the detection error when using System 3 and 4 are tabulated in Tables VI and VII, respectively. The measured error of the estimated positive- and negative-sequence components of the grid voltage when using System 3 and 4 are plotted in Figs. 14 and 15, respectively. The measurement results confirm the calculations above. In Fig. 15, only the error introduced by the PLL can be observed in the measured errors.

For System 3, the error in the estimated sequence components is reduced compared with System 1 (see Table IV). The oscillatory term is reduced by about one third for both sequences. However, the offsets are still not zero and it can be noticed that both $\Delta e_{\mathrm{pdav,off}}^{(dqp)}$ and $\Delta e_{\mathrm{nqav,off}}^{(dqn)}$ have increased compared with the values obtained using System 1. As expected, a better estimation can be achieved by using weighted mean average of the error. From Table VII, it can be observed that both the constant and the oscillatory terms of the error have been drastically reduced as compared with System 1 and 3, with the exception of $\Delta e_{\mathrm{pdw,off}}^{(dqp)}$, which is still slightly higher as compared with the value obtained for System 1.

Finally, Fig. 16 shows a comparison between measured and calculated amplitude of the relative estimation error when the

TABLE VI
DSC Parameters and Calculated Detection Errors for Study Case With Unbalanced Voltage, System 3

$\lambda_{\mathrm{av}} = 0.62\%$				$\gamma_{\mathrm{av}} = 357.4°$	
Positive sequence					
$\Delta e_{\mathrm{pdav,off}}^{(dqp)}$	-0.03%	$\Delta e_{\mathrm{pdav,osc}}^{(dqp)}$	0.04%	δ_{pdav}	$359.8°$
$\Delta e_{\mathrm{pqav,off}}^{(dqp)}$	-0.56%	$\Delta e_{\mathrm{pqav,osc}}^{(dqp)}$	0.04%	δ_{pqav}	$269.8°$
Negative sequence					
$\Delta e_{\mathrm{ndav,off}}^{(dqn)}$	0.04%	$\Delta e_{\mathrm{ndav,osc}}^{(dqn)}$	0.56%	δ_{ndav}	$87.4°$
$\Delta e_{\mathrm{nqav,off}}^{(dqn)}$	-0.003%	$\Delta e_{\mathrm{nqav,osc}}^{(dqn)}$	0.56%	δ_{nqav}	$177.4°$

TABLE VII
DSC Parameters and Calculated Detection Errors for Study Case With Unbalanced Voltage, System 4

$\lambda_{\mathrm{w}} = 0.02\%$				$\gamma_{\mathrm{w}} = 269.5°$	
Positive sequence					
$\Delta e_{\mathrm{pdw,off}}^{(dqp)}$	-0.02%	$\Delta e_{\mathrm{pdw,osc}}^{(dqp)}$	0.001%	δ_{pdw}	$87.7°$
$\Delta e_{\mathrm{pqw,off}}^{(dqp)}$	$\simeq 0\%$	$\Delta e_{\mathrm{pqw,osc}}^{(dqp)}$	0.001%	δ_{pqw}	$357.7°$
Negative sequence					
$\Delta e_{\mathrm{ndw,off}}^{(dqn)}$	$\simeq 0\%$	$\Delta e_{\mathrm{ndw,osc}}^{(dqn)}$	0.02%	δ_{ndw}	$359.5°$
$\Delta e_{\mathrm{nqw,off}}^{(dqn)}$	-0.001%	$\Delta e_{\mathrm{nqw,osc}}^{(dqn)}$	0.02%	δ_{nqw}	$89.5°$

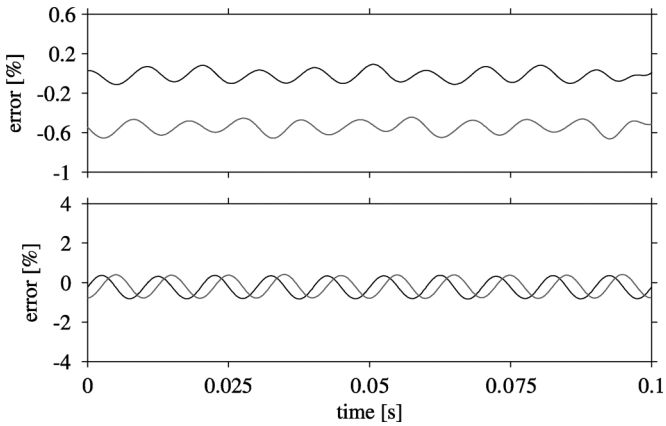

Fig. 14. Measured error in phase-sequence estimation during unbalanced steady-state voltage using System 3 $f_{\mathrm{g}} = 50$ Hz, $f_{\mathrm{s}} = 5060$ Hz. Top: positive-sequence components in positive SRF (black: d-component; red: q-component). Bottom: negative-sequence components in negative SRF (black: d-component; red: q-component).

$$\lambda_{\mathrm{w}} = \sqrt{\left(\frac{\Delta n - 1}{2}\cos\upsilon_1 - \frac{\Delta n}{2}\cos\upsilon_2\right)^2 + \left[\frac{1-\Delta n}{2}(\sin\upsilon_1 - 1) + \frac{\Delta n}{2}(\sin\upsilon_2 - 1)\right]^2} \quad (42)$$

$$\gamma_{\mathrm{w}} = \arctan\left(\frac{a\lambda_1\sin\gamma_1 + (1-a)\lambda_2\sin\gamma_2}{a\lambda_1\cos\gamma_1 + (1-a)\lambda_2\cos\gamma_2}\right) \quad (43)$$

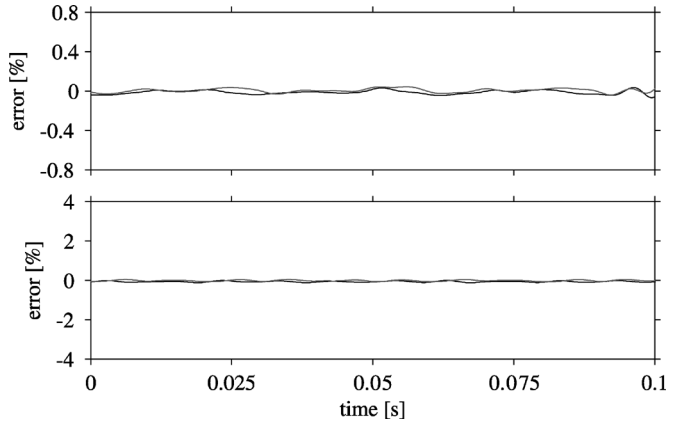

Fig. 15. Measured error in phase-sequence estimation during unbalanced steady-state voltage using System 4, $f_{\mathrm{g}} = 50$ Hz, $f_{\mathrm{s}} = 5060$ Hz. Top: Positive sequence components in positive SRF (black: d-component; red: q-component). Bottom: Negative sequence components in negative SRF (black: d-component; red: q-component).

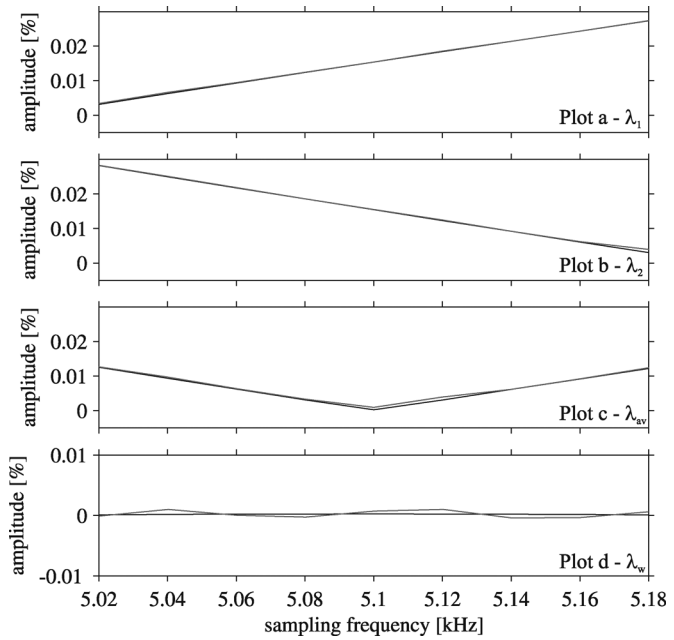

Fig. 16. Comparison between calculated (black) and measured (red) amplitude of relative estimation error when using System 1 (Plot a), System 2 (Plot b), System 3 (Plot c), and System 4 (Plot d).

sampling frequency is varied between 5.02 and 5.18 kHz using System 1 (λ_1, Plot a), System 2 (λ_2, Plot b), System 3 (λ_{av}, Plot c) and System 4 (λ_{w}, Plot d). The measurement results confirm the analytical models very well. Only a small difference in the measurement results (more evident for λ_{w}, due to the lower scale of the figure), due to the nonideal grid voltage, can be observed.

VII. Grid Frequency Influence on DSC

In this section, the influence of the grid frequency on DSC is studied. The grid frequency always fluctuates. However, for a stiff grid, the fluctuation is normally small. Exceptionally, during major grid disturbances or in island grids, large fluctuations in the grid frequency can be experienced and, therefore, it can be of interest to study their influence on the DSC method. Equation (1) describes the grid voltage vector in the $\alpha\beta$-plane in the generic case of unsymmetric grid and in continuous time domain. The angular frequency ω_{g} can be written as

$$\omega_{\mathrm{g}} = 2\pi f_{\mathrm{g}} = 2\pi(f_{\mathrm{g0}} + \Delta f_{\mathrm{g}}) \tag{46}$$

where f_{g0} and Δf_{g} are nominal frequency and frequency deviation, respectively. The grid period can be written as

$$T_{\mathrm{g}} = 1/f_{\mathrm{g}} = T_{\mathrm{g0}} + \Delta T_{\mathrm{g}} \tag{47}$$

yielding

$$\Delta T_{\mathrm{g}}/T_{\mathrm{g}} = -\Delta f_{\mathrm{g}}/f_0. \tag{48}$$

The separation method uses the nominal grid period in order to separate the positive and the negative phase sequence components. Using (47) in (2), the estimated positive-sequence voltage in the $\alpha\beta$-coordinate system becomes

$$\hat{\underline{e}}_{\mathrm{p}}^{(\alpha\beta)}(t) = E_{\mathrm{p}}\lambda \mathrm{e}^{\mathrm{j}\left(\omega_{\mathrm{g}}t - \frac{\pi}{2} + \varphi_{\mathrm{p}} + \gamma\right)} + E_{\mathrm{n}}\lambda \mathrm{e}^{-\mathrm{j}\left(\omega_{\mathrm{g}}t - \frac{\pi}{2} + \varphi_{\mathrm{n}} + \gamma\right)} \tag{49}$$

where

$$\lambda = \sqrt{\frac{1}{2}\left(1 - \cos\left(\frac{\pi}{2}\kappa_{\mathrm{T}}\right)\right)} \tag{50}$$

and

$$\gamma = \arctan\left[\frac{\cos\left(\frac{\pi}{2}\kappa_{\mathrm{T}}\right) - 1}{\sin\left(\frac{\pi}{2}\kappa_{\mathrm{T}}\right)}\right] \tag{51}$$

with κ_{T} the relative grid period error, defined by

$$\kappa_{\mathrm{T}} = \Delta T_{\mathrm{g}}/T_{\mathrm{g}}. \tag{52}$$

Analogously, substituting from (47) into (3), the negative phase-sequence component becomes

$$\hat{\underline{e}}_{\mathrm{n}}^{(\alpha\beta)}(t) = \underline{e}_{\mathrm{n}}^{(\alpha\beta)}(t) + E_{\mathrm{p}}\lambda \mathrm{e}^{\mathrm{j}\left(\omega_{\mathrm{g}}t - \frac{\pi}{2} + \varphi_{\mathrm{p}} + \gamma\right)} + \underline{e}_{\mathrm{n}}^{(\alpha\beta)}(t) + E_{\mathrm{n}}\lambda \mathrm{e}^{-\mathrm{j}\left(\omega_{\mathrm{g}}t - \frac{\pi}{2} + \varphi_{\mathrm{n}} + \gamma\right)}. \tag{53}$$

As shown in (49) and (53), the error due to grid frequency deviation has the same expression as the error due to nonideal discretization. Hence, the previous derivations can be applied to this case without any modifications. Thus, the previous figures can be reused in order to determine the estimation errors.

VIII. Conclusion

In this paper, the use of a method for online detection of positive- and negative-sequence components of three-phase quantities, named the delayed signal cancellation (DSC) method, has been investigated.

It has been shown that in practical implementation of the method in a computer-controlled system, a detection error may arise due to nonideal discretization, unless the sampling frequency can be chosen to be in a specific relation with the

grid frequency, which is normally not the case. Analytical expressions of the error have been derived and calculations have been verified experimentally via three-phase grid voltage measurements obtained with a state-of-the-art digital signal processor (DSP) system. Both cases of balanced and unbalanced grid voltage have been shown.

Furthermore, two methods have been presented to reduce the detection error. Key equations for both methods have been derived and again verified experimentally. It has been shown that the method based on weighted averaging allows achieving a drastic reduction of the detection error.

Finally, since the DSC method relies on accurate knowledge of the grid frequency, the effect of grid frequency variations has been considered. It has been demonstrated that the error due to inaccurate knowledge of the grid frequency and the error due to nonideal discretization have the same expression and, therefore, the given derivations, including the proposed methods for reducing the detection errors, can be applied without modifications to the case of grid frequency variations.

REFERENCES

[1] M. H. J. Bollen, *Understanding Power Quality Problems: Voltage Sags and Interruptions*. New York: IEEE Press, 1999.

[2] G. Saccomando, J. Svensson, and A. Sannino, "Improving voltage disturbance rejection for variable-speed wind turbines," *IEEE Trans. Energy Convers.*, vol. 17, no. 3, pp. 422–428, Sep. 2002.

[3] P. Rioual, H. Pouliquen, and J. P. Louis, "Regulation of a PWM rectifier in the unbalanced network state using a generalized model," *IEEE Trans. Power Electron.*, vol. 11, no. 3, pp. 495–502, May 1996.

[4] G. Saccomando and J. Svensson, "Transient operation of grid-connected voltage source converter under unbalanced voltage conditions," in *Proc. IEEE Industry Applications Soc. 36th Annu. Meeting*, Sep. 2001, vol. 4, pp. 2419–2424.

[5] T. N. Le, "Kompensation schnell veranderlicher Blindstrome eines Drehstromverbrauchers," (in German) *EtzArchiv*, vol. Bd. 11, no. H. 8, pp. 249–253, 1989.

[6] T. Larsson and C. Poumarede, "STATCOM, an efficient means for flicker mitigation," in *Proc. IEEE Power Eng. Soc. Winter Meeting*, Jan./Feb. 1999, vol. 2, pp. 1208–1213.

[7] H. Awad, J. Svensson, and M. H. J. Bollen, "Mitigation of unbalanced voltage dips using static series compensator," *IEEE Trans. Power Electron.*, vol. 19, no. 3, pp. 837–846, May 2004.

[8] F. A. Magueed, A. Sannino, and J. Svensson, "Transient performance of voltage source converter under unbalanced voltage dips," in *Proc. IEEE 35th Annu. Power Electronics Specialists Conf.*, Jun. 2004, vol. 2, pp. 1163–1168.

[9] dSPACE, Solutions for Control [Online]. Available: http://www.dspace.de/ww/en/pub/home.htm.

[10] L. Harnefors, "Control of variable-speed drives," Ph.D. dissertation, Applied Signal Processing and Control, Dept. Electron., Mälardalen Univ, Västerås, Sweden, 2002.

[11] R. Ottersten, "On control of back-to-back converters and sensorless induction machine drives," Ph.D. dissertation, Chalmers Univ. Technol., Göteborg, Sweden, Jun. 2003.

[12] S.-K. Chung, "A phase tracking system for three phase utility interface inverters," *IEEE Trans. Power Electron.*, vol. 15, no. 3, pp. 431–438, May 2000.

Jan Svensson (S'96–M'98) received the M.Sc., Lic. Eng., Ph.D., and D.Sc. degrees from Chalmers University of Technology, Göteborg, Sweden, in 1991, 1995, 1998, and 2002, respectively.

From 1998 to 2002, he was an Assistant Professor in the Department of Electric Power Engineering, Chalmers University of Technology. Currently, he is with ABB Power Technologies, Västerås, Sweden, involved in development of FACTS and HVDC transmission, especially in design and control of light-concept devices. His interests include control of power electronics in power systems, power quality, and wind power.

Massimo Bongiorno (S'02) received the M.Sc. degree in electrical engineering from the University of Palermo, Palermo, Italy, in 2002 and the Lic.Eng. degree from Chalmers University of Technology, Göteborg, Sweden, in 2004, where he is currently pursuing the Ph.D. degree.

His interests include application of power electronics in power systems and power quality.

Ambra Sannino (S'99–M'01) received the M.Sc. and Ph.D. degrees in electrical engineering from the University of Palermo, Palermo, Italy, in 1997 and 2001, respectively, and the D.Sc. degree in power systems from Chalmers University of Technology, Göteborg, Sweden, in 2003.

From 2001 to 2004, she was an Assistant Professor and Associate Professor with the Department of Electric Power Engineering, Chalmers University of Technology. Since 2004, she has been with ABB Corporate Research, Västerås, Sweden. Her interests include applications of power electronics in power systems, distributed generation, wind power, and power quality.